

# A Software Technique for Flow-Rate Measurement in Horizontal Two-Phase Flow

T.D. Darwich,\* SPE, Haluk Toral, and J.S. Archer, SPE, Imperial C.

SPE 19510

**Summary.** This paper presents a software technique for measuring individual phase flow rates in two-phase flow. The technique is based on the extraction, classification, and identification of stochastic features from turbulent pressure and void-fraction waveforms. Experiments in a horizontal air/water loop showed that a set of stochastic features is uniquely related to the individual phase flow rates. The software flowmeter is calibrated in situ by compilation of feature sets related to individual phase flow rates in a data base. On-line flow-rate measurement is made by a pattern recognition technique that identifies the best match to the measured feature vector from the calibration data base.

## Introduction

In the current practice for testing multiphase well and pipe flow, a test separator separates different fluid phases, which are then metered in their respective single-phase flowlines by any single-phase flow measurement device. This approach suffers from inaccuracy and high cost.

The requirements for a multiphase meter include an accuracy of  $\pm 5\%$  for reservoir management and  $\pm 0.5\%$  for fiscal measurement, a small footprint, minimum length upstream and downstream of the meter, a sampling frequency of at least 10 Hz, design pressure up to 35 MPa, and a pressure drop of not more than 100 kPa across the meter. Finally, the meter should be easy to install and maintain.<sup>1</sup>

The software-based multiphase metering technique (called ESMER) reported in this paper appears to offer an accuracy suitable for testing and to meet the design criteria for an oilfield on-line multiphase flowmeter (Fig. 1).

## Theoretical Background

**Stochastic Features.** A number of researchers<sup>2-11</sup> used stochastic methods to analyze pressure and void-fraction waveforms to discriminate between different flow regimes. We have extended the stochastic treatment of the turbulent pressure and void-fraction waveforms by applying signal analysis methods, such as voice recognition, used in other disciplines. These methods have enabled us to derive "stochastic features" that characterize flow regimes with a greater degree of sensitivity and reproducibility than previously available.

The stochastic features can be separated into two groups, the amplitude- and frequency-domain features. The amplitude-domain features include the probability density function, standard deviation, coefficient of skewness, and kurtosis. The frequency-domain features, widely used in voice and speaker recognition research, include the linear prediction coefficients.<sup>12,13</sup>

**Feature Vector.** A set of stochastic features derived from a waveform is called the "feature vector" of the waveform. We can also visualize the waveform as a distinct "object" by translating its feature vector to "feature space," as shown in Fig. 2. We use "waveform" to mean any signal that can be obtained from any sensor or combination of sensors that responds to the turbulent hydrodynamics of the flow, such as pressure, differential pressure, and void-fraction sensors.

**Flow-Regime Maps.** Many studies propose generalized multiphase flow-regime maps on the basis of empirical/visual observations<sup>14-16</sup> and/or mechanistic force balances.<sup>17,18</sup>

**Flow-Regime/Rate-Identification Grid.** The superficial-velocity flow-regime map is used in this study. This map is overlain by a

grid, and we propose that each grid cell has a unique hydrodynamic waveform that can be modeled by its feature vector. Grid cells can be refined, depending on the variation of the feature vector between adjacent cells. This variation must be greater than the variation of the feature vector within a given grid cell in consecutive measurements (under conditions of constant superficial velocity).

**F-Ratio.** An objective scale, the *F*-ratio, can be established to test the sensitivity of the feature vector to distinguish between neighboring cells. Atal<sup>19</sup> first used the *F*-ratio in speaker recognition. It was defined as:

$$F = \frac{\text{variance of speaker means}}{\text{average of individual speaker variance}},$$

$$\text{or } F = \frac{\langle (\bar{x}_i - \bar{\mu})^2 \rangle_i}{\langle (x_{\alpha}^i - \bar{x}_i)^2 \rangle_{\alpha,i}},$$

where  $x$ =time dependent quantity observed,  $\langle \cdot \rangle_i$ =average over speakers,  $\langle \cdot \rangle_{\alpha}$ =average over different blocks of one speaker,  $\bar{x}_i = \langle x_{\alpha}^i \rangle_{\alpha}$ ,  $\alpha$ =block of observation, and  $\bar{\mu} = \langle \bar{x}_i \rangle_i$ . The higher the *F*-ratio, the greater the chances of speaker identification.

ESMER's two-phase grid nodes are analogous with speakers; i.e., ESMER identifies grid nodes by the same techniques used to identify speakers. Speaker recognition techniques "train" the recognition system on the digitized waveforms of the voices or utterances of the speakers. ESMER trains (calibrates) the recognition system on the digitized waveforms of the turbulent hydrodynamic signals.

The capabilities of the pattern recognition algorithms notwithstanding, the higher the *F*-ratio, the greater the refinement of the grid cells; i.e., the greater the sensitivity of the technique to flow-regime or flow-rate identification. At its coarsest, ESMER is capable of identifying flow regimes. Beyond a certain threshold, grid-cell identification can be related directly to individual phase flow rates.

The strength of the *F*-ratio is expected to depend on a number of factors, such as sensor selection, number of calibration points, stochastic features derived from the flow, flowline geometry (up- and downstream conditions, diameter, and orientation), and fluid physical properties.

**Calibration.** ESMER must be calibrated in situ by extraction of feature vectors at a number of grid cells. Contour mapping techniques are used to interpolate/extrapolate the measurements to the entire grid-cell domain. The adequacy of the calibration points can be determined through observation of (1) the variance of the contour map with additional data (Fig. 3) or (2) the change in *F*-ratio with additional gridpoints.

**Pattern Recognition.** Flow regime and rates are identified by matching measured feature vectors to those in the calibration data

\*Now at Cairo U.

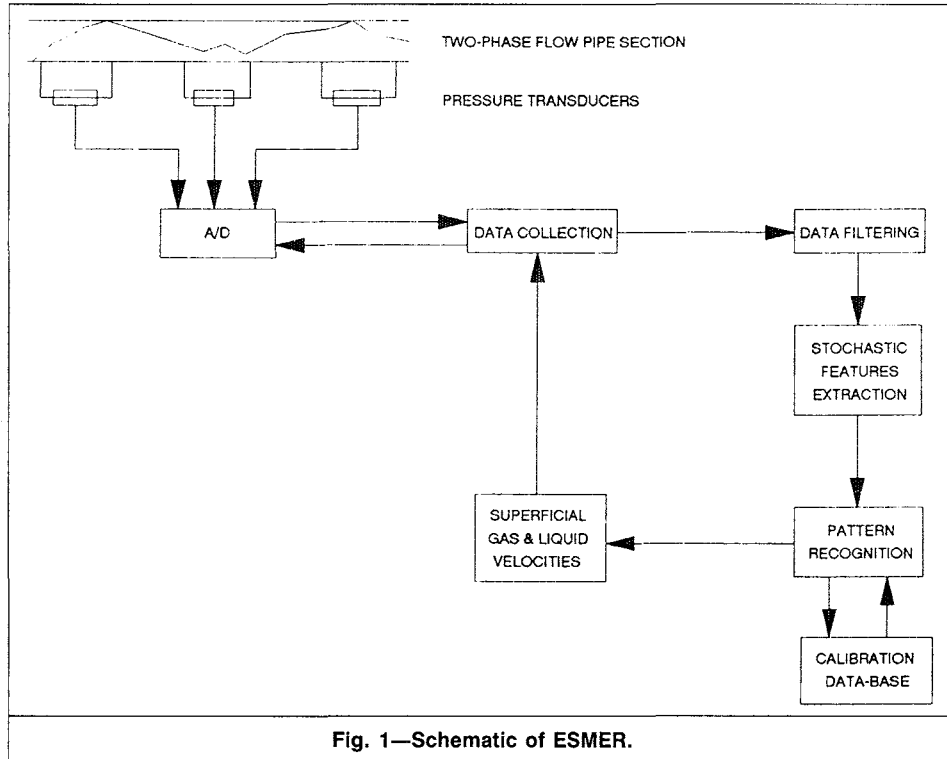


Fig. 1—Schematic of ESMER.

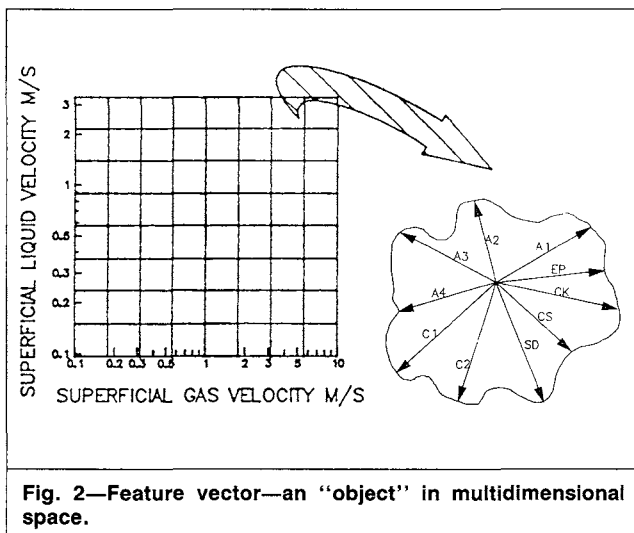


Fig. 2—Feature vector—an “object” in multidimensional space.

base. In this study, the Euclidean distance template matching technique was used. With this technique, the match is quantified by

$$D_e = \sum_{i=1}^n \left[ \frac{(M_i - C_i)}{s_i} \right]^2,$$

where  $D_e$  is the Euclidean distance between the measured vector,  $M$ , and the calibration pattern,  $C$ .  $M_i$  and  $C_i$  are the  $i$ th feature of the measured and calibration feature vectors, and  $n$  is the number of features in the vector set.  $s_i$  is the standard deviation of the  $i$ th feature used to normalize the feature domains.

**Software Package.** A user-friendly software package was developed that contained facilities for multichannel digital data acquisition, digital filter design and implementation, time- and frequency-domain displays of the digitized signal, interactive or automated calibration, contour mapping of feature vectors, and online measurement with an analog representation of the individual phase flow rates.<sup>20</sup>

## Experiments

**Test Rig.** Fig. 4 is a schematic of the horizontal two-phase flow loop. Water flow rate was measured with an orifice; compressed-air flow rate was measured with a rotameter or an orifice. Two separate 8.8-m-long test sections of 50- and 26-mm-diameter pipe, with stabilization lengths of 113 and 217 times the diameter, respectively, were used. Table 1 shows the range of flow rates. All flow regimes except annular flow were tested. Measurements were made at atmospheric pressure.

**Sensors.** Two absolute-pressure and three differential-pressure transducers, a void-fraction capacitance transducer, and a conductance microprobe were used. Differential-pressure tappings were configured radially and axially. Darwiche<sup>21</sup> described the conductance and capacitance probes in detail.

**Data-Acquisition System.** Measurements were digitized with an analog-to-digital (A/D) converter controlled by a PC. The 8-channel, 12-bit A/D converter was capable of sampling at frequencies up to 20 kHz. Digital-filtering software allowed the design and implementation of low-pass, high-pass, band-pass, and band-stop recursive or nonrecursive filters to isolate the extraneous noise from sampled waveforms. The spectral densities of the signals were displayed to determine the optimum sampling frequency and to record lengths.

## Results and Discussion

This section describes the application of the ESMER technique to the horizontal air/water flow loop described earlier.

**Calibration.** Waveforms were sampled and analyzed on 545 points in the 50-mm pipe and 370 points in the 26-mm pipe. Each measurement comprised 4,096 sample points, which were divided into 16 blocks of 256 points each to ensure that statistical properties were stationary across the waveforms. Time- and frequency-domain variations of the waveforms were studied graphically to detect extraneous noise. Noise was eliminated by digital filtering.

The following feature vector was derived from each waveform:

$$[s \ S \ K \ V_p \ a_1 \ a_2 \ a_3 \ a_4],$$

where the amplitude-domain features are standard deviation,  $s$ , coefficient of skewness,  $S$ , and coefficient of kurtosis,  $K$ . The

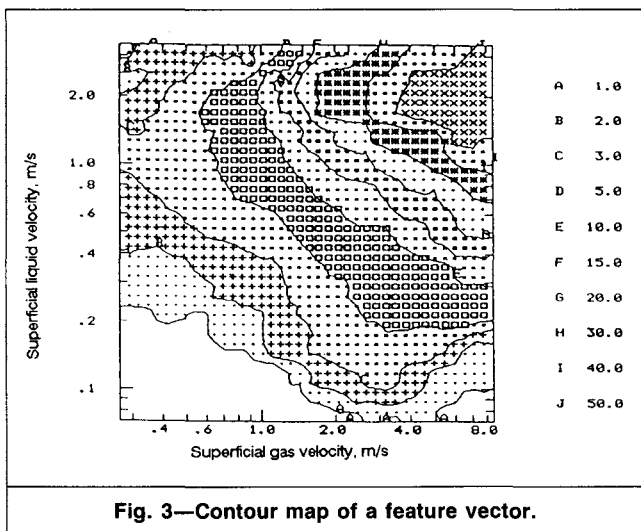


Fig. 3—Contour map of a feature vector.

frequency-domain features are linear prediction residual error coefficient,  $V_p$ , and linear prediction coefficients,  $a_1$  through  $a_4$ .

The preliminary study of the stationarity of the waveforms was made by plotting the average value of the features within a sample block of 256 points over 16 blocks (Fig. 5). Feature-vector measurements were surface fitted over a  $40 \times 40$  regular grid cell by contouring techniques. Fig. 6 shows examples of the feature-vector contour maps for the radial differential-pressure signal.

Feature-vector strength with respect to waveform and individual features was quantified by the  $F$ -ratio test. Table 2 shows the  $F$ -ratio for the absolute- and differential-pressure signals in the 50-mm pipe. These were found to have a higher  $F$ -ratio than other sensors used in this study.<sup>21</sup>

Darwiche<sup>21</sup> showed the effect of pipe diameter on the feature vectors by comparing the measurements conducted on 50- and 26-mm-diameter pipes. Generally, it was observed that the feature maps showed similar trends but that isolines did not coincide. Thus,

TABLE 1—RANGE OF FLOW RATES

ID (mm)	Superficial Water Velocity (m/s)	Superficial Air Velocity (m/s)
50	0.072 to 3.405	0.266 to 8.509
26	0.282 to 3.360	0.115 to 8.621

calibration depends on pipe diameter if superficial velocities alone are chosen as the key fields in the calibration data base.

**Measurement.** The template matching categorizer was tested with 129 measurements in the 50-mm pipe chosen at random over the whole flow domain. The effect of feature-vector size was investigated through use of the following feature sets: absolute pressure with eight features; differential pressure with eight features; and absolute and differential pressure combined with 16 features. It was observed that the combined feature vector resulted in considerable improvement in recognition rate (Fig. 7). Five different measures of error were used<sup>15</sup>:

$$\begin{aligned} \mathcal{E}_1 &= \left( \frac{1}{n} \sum_{i=1}^n e_i^2 \right)^{\frac{1}{2}}, \\ \mathcal{E}_2 &= \frac{1}{n} \sum_{i=1}^n |e_i|, \\ \mathcal{E}_3 &= \frac{1}{n} \sum_{i=1}^n e_i, \\ \mathcal{E}_4 &= \frac{100}{n} \sum_{i=1}^n \left| \frac{e}{v_a} \right|_i, \\ \text{and } \mathcal{E}_5 &= \frac{100}{n} \sum_{i=1}^n \left( \frac{e}{v_a} \right)_i, \end{aligned}$$

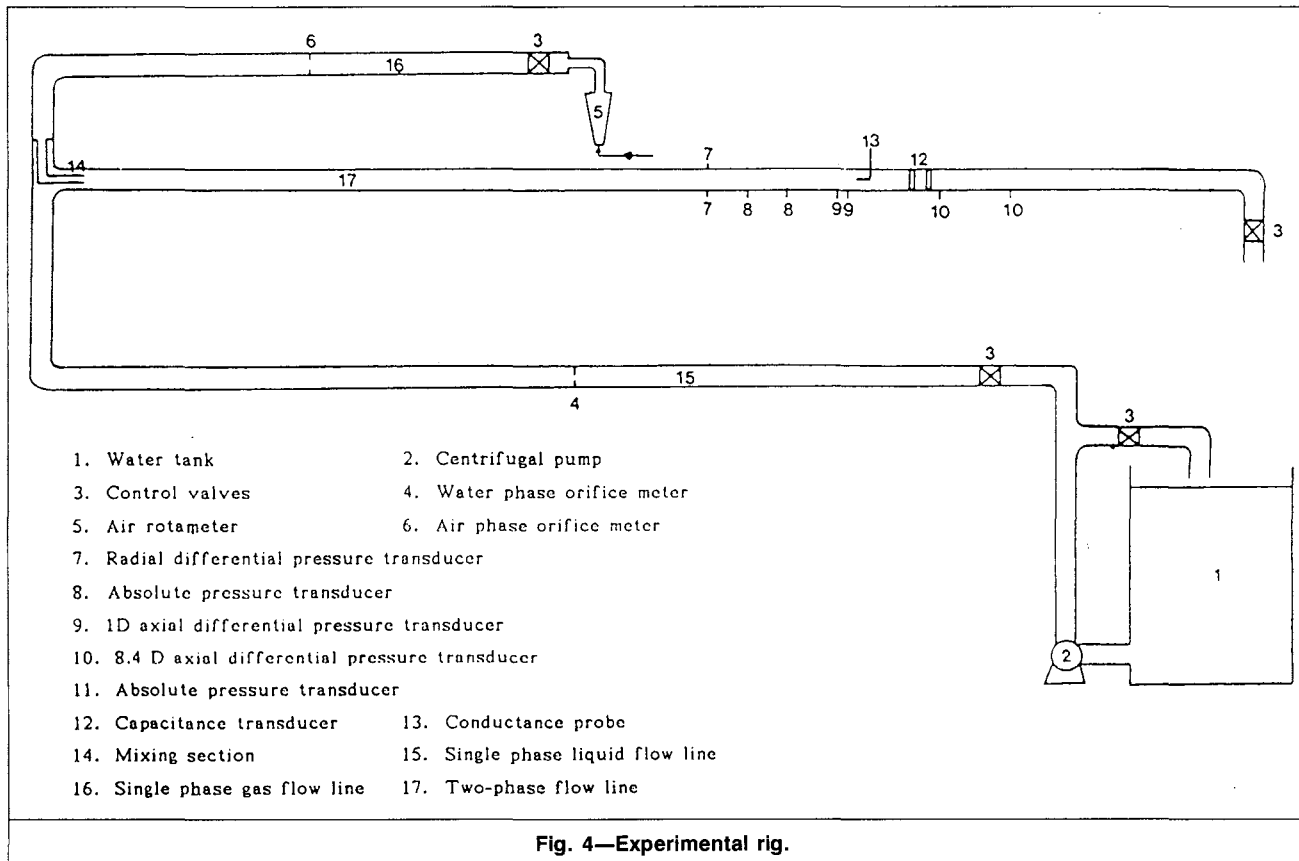


Fig. 4—Experimental rig.

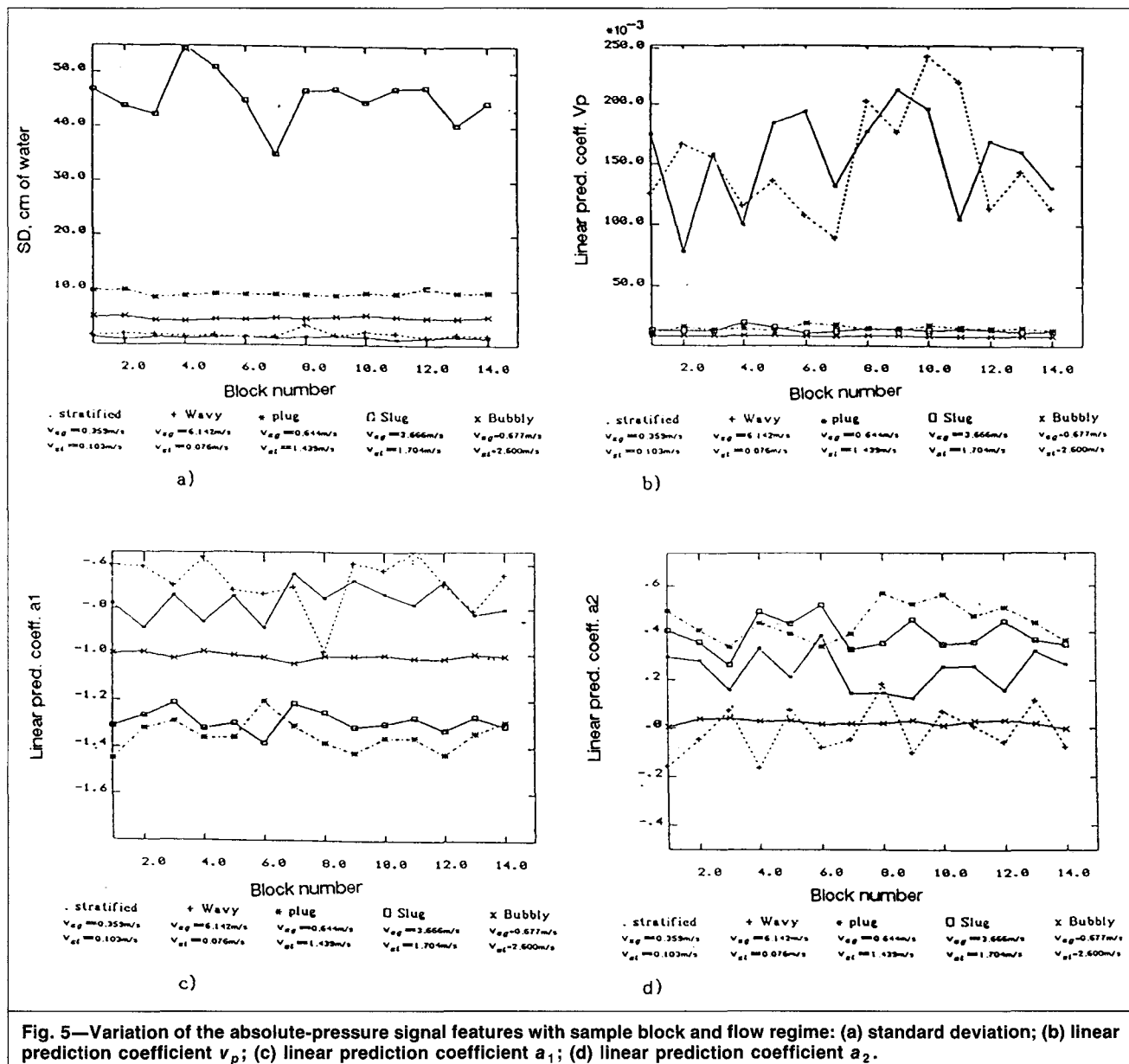


Fig. 5—Variation of the absolute-pressure signal features with sample block and flow regime: (a) standard deviation; (b) linear prediction coefficient  $v_p$ ; (c) linear prediction coefficient  $a_1$ ; (d) linear prediction coefficient  $a_2$ .

TABLE 2—F-RATIO OF ABSOLUTE- AND DIFFERENTIAL-PRESSURE SIGNAL FEATURES

Features	F-ratios			
	Absolute Pressure	Radial Differential	Axial Differential	
			1D	8.4D
S	29.00	53.20	39.60	60.50
S	2.00	0.28	0.12	1.66
K	0.63	0.76	0.53	1.18
$v_p$	2.90	5.09	3.42	2.79
$a_1$	5.30	5.48	6.29	2.01
$a_2$	4.00	2.23	6.61	1.15
$a_3$	2.00	0.95	2.21	0.57
$a_4$	1.90	2.10	4.07	0.94

where  $e_i = (v_m - v_a)_i$ ,  $v_m$  = measured (i.e., the recognized) superficial velocity, and  $v_a$  = actual superficial velocity.

Consider the following to understand the need for different measures of error.

1. An additional error measure is defined here as

$$\mathcal{E}_6 = 100[e/(v_{\max} - v_{\min})]_i$$

where  $(v_{\max} - v_{\min})$  is the difference between maximum and minimum velocities (i.e., the measurable flow range). We found that for 96% of the gas-velocity measurements,  $\mathcal{E}_6$  lay within  $\pm 10\%$  range; it was within  $\pm 5\%$  range for 87% of the measurements. For liquid-velocity measurements, 95% of measurements lay within  $\pm 10\%$  and 85% within  $\pm 5\%$ .

2.  $\mathcal{E}_1$  is sensitive to errors at high velocities.
3.  $\mathcal{E}_2$  is sensitive to errors at low velocities.
4.  $\mathcal{E}_3$  provides overall accuracy with positive and negative deviations canceling each other.
5.  $\mathcal{E}_4$  and  $\mathcal{E}_5$  are sensitive to errors at low velocity.

**Tables 3 and 4** show the value of the various error measures in gas- and liquid-velocity measurements with different feature vectors.

### Conclusions

1. The superficial gas/liquid-velocity surface can be divided into grid cells where each cell can be uniquely characterized by a stochastic feature vector derived from the turbulent hydrodynamic waveforms sampled at high frequencies.
2. The relative strength of features can be assessed by the F-ratio test. In air/water horizontal flow, the strongest features were derived from absolute- and differential-pressure waveforms.

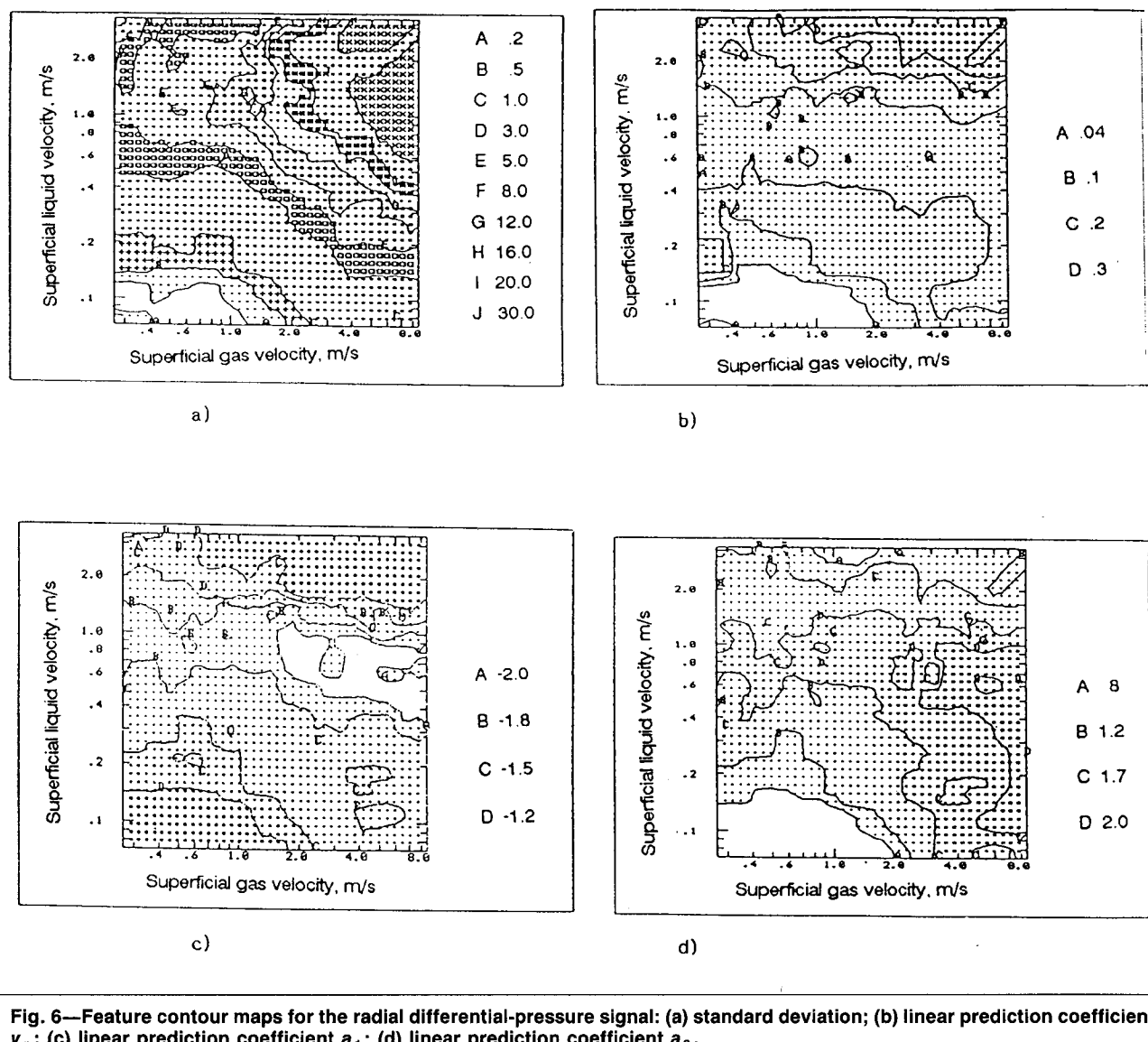


**Fig. 6—Feature contour maps for the radial differential-pressure signal: (a) standard deviation; (b) linear prediction coefficient  $v_p$ ; (c) linear prediction coefficient  $a_1$ ; (d) linear prediction coefficient  $a_2$ .**

**TABLE 3—COMPARISON OF SYSTEM PERFORMANCE IN SUPERFICIAL-GAS-VELOCITY MEASUREMENT**

Error Parameter	Differential-Pressure Signal	Absolute-Pressure Signal	Both Signals
$\epsilon_1$	1.005	0.578	0.425
$\epsilon_2$	0.483	0.317	0.248
$\epsilon_3$	-0.072	-0.079	-0.043
$\epsilon_4$	26.363	19.344	15.019
$\epsilon_5$	4.794	-2.137	-0.066

3. Individual phase velocities can be measured by a template matching pattern recognition technique, which obtains a match between the measured vector and the calibration set.

4. The technique is implemented by a user-friendly software package that can be installed on flowlines with minimum alteration and cost because it works with proprietary sensors.

5. The technique can be extended to oil/water/gas three-phase flow with the following advantages: it enhances the feature vector by the addition of further frequency-domain features; it uses other sensors sensitive to the hydrodynamic/physical properties of the three phases (i.e., in addition to the current pressure sensors); and it uses pattern recognition techniques that consider the sensitivity of the feature vectors to flow regime and compensate for the relative strengths of the features by weighting coefficients.

**TABLE 4—COMPARISON OF SYSTEM PERFORMANCE IN SUPERFICIAL-LIQUID-VELOCITY MEASUREMENT**

Error Parameter	Differential-Pressure Signal	Absolute-Pressure Signal	Both Signals
$\epsilon_1$	0.256	0.199	0.146
$\epsilon_2$	0.151	0.121	0.092
$\epsilon_3$	0.029	0.063	0.023
$\epsilon_4$	19.399	14.188	7.408
$\epsilon_5$	9.551	7.602	1.377

## References

1. Ashkuri, S. and Hill, T.J.: "Measurement of Multiphase Flows in Crude Oil Production Systems," *Pet. Rev.* (Nov. 1985) 14-16.
2. Hubbard, M.G. and Dukler, A.E.: "The Characterization of Flow Regimes for Horizontal Two-Phase Flow," *Proc., Heat Transfer and Fluid Mechanics Inst.* (1966) 100-21.
3. Nishikawa, K., Sekoguchi, K., and Fukano, T.: "On the Pulsation Phenomena in Gas-Liquid Two-Phase Flow (Relationship Between Pulsating Pressure and Flow Pattern in Upward Two-Phase Flow)," *Bull., J. Soc. Mechanical Eng.* (Dec. 1969) **12**, No. 54, 1410-16.
4. Jones, O.C. and Zuber, N.: "The Interrelation Between Void Fraction Fluctuations and Flow Patterns in Two-Phase Flow," *Int. J. Multiphase Flow* (1975) **2**, No. 1, 273-306.
5. Matsui, G.: "Identification of Flow Regimes in Vertical Gas-Liquid Two-Phase Flow Using Differential Pressure Fluctuations," *Int. J. Multiphase Flow* (1984) **10**, No. 6, 711-20.

## Authors



Darwich



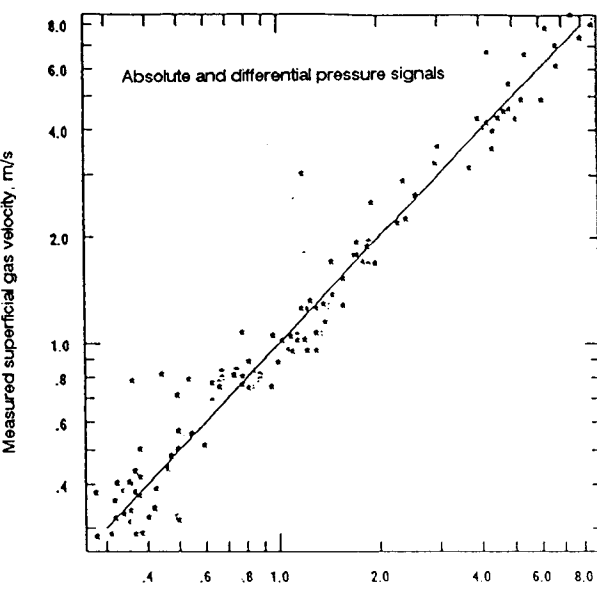
Archer



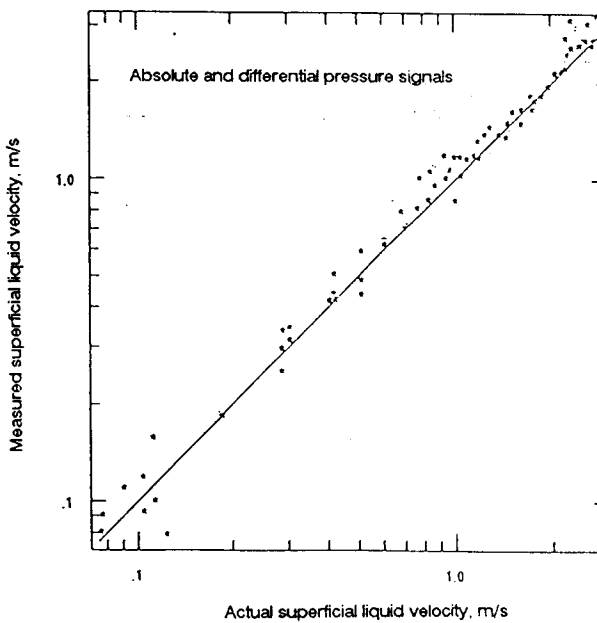
Toral

**Tarek D. Darwich** is an assistant professor of petroleum engineering at Cairo U. He previously was an assistant professor at Kuwait U. and an analyst for W.S. Atkins Engineering Sciences in England. He holds BSc and MSc degrees from Cairo U. and DIC and PhD degrees from Imperial C., all in petroleum engineering. **Haluk Toral**, a lecturer in the Dept. of Mineral Resources Engineering at Imperial C. of Science and Technology, has research interests in software applications and multiphase flowmetering. He holds BSc and PhD degrees in chemical engineering. **J.S. Archer** is a professor of petroleum engineering, head of the Dept. of Mineral Resources Engineering, dean of the Royal School of Mines, and pro-rector designate at Imperial C. His research interests include petroleum reservoir characterization and numerical modeling of multiphase flow processes.

6. Matsui, G.: "Identification of Flow Patterns in Horizontal Gas-Liquid Two-Phase Flow Using Differential Pressure Fluctuations," *Proc., Intl. Symposium on Fluid Control and Measurement*, Tokyo (1985) 819-22.
7. Matsui, G.: "Automatic Identification of Flow Regimes in Vertical Two-Phase Flow Using Differential Pressure Fluctuations," *Nuclear Engineering and Design* (1986) **95**, 221-31.
8. Annunziato, M. and Girardi, G.: "Flow Pattern Identification by Pressure Drop and Void Fraction Fluctuations Analysis in Vertical Two-Phase Flow," *Proc., European Two-Phase Flow Group Meeting*, Rome (June 19-21, 1983) paper F4.
9. Annunziato, M. and Girardi, G.: "Statistical Methods to Identify Two-Phase Regimes: Experimental Results for Vertical Large Diameter Tubes," *Proc., Second Intl. Conference on Multiphase Flow*, London (June 19-21, 1985) paper G5.
10. Annunziato, M. and Girardi, G.: "Horizontal Two-Phase Flow: A Statistical Method for Flow Pattern Recognition," *Proc., Third Intl. Conference on Multiphase Flow*, The Hague (May 18-20, 1987) 169-85.
11. Sekoguchi, K., Inoue, K., and Imasaka, T.: "Void Signal Analysis and Gas-Liquid Two-Phase Flow Regime Determination by a Statistical Pattern Recognition Method," *JSME Intl. J.* (Aug. 1987) **30**, No. 266, 1266-73.
12. Atal, B.S. and Hanauer, S.L.: "Speech Analysis and Synthesis by Linear Prediction of the Acoustic Wave," *J. Acoust. Soc. Amer.* (1971) **50**, No. 2, 637-55.
13. Makhoul, J.: "Linear Prediction: A Tutorial Review," *Proc., IEEE* (April 1975) **63**, No. 4, 561-80.
14. Baker, O.: "Design for Simultaneous Flow of Oil and Gas," *Oil & Gas J.* (1954) **53**, No. 12, 185-95.
15. Mandhane, J.M., Gregory, G.A., and Aziz, K.: "A Flow Pattern Map for Gas-Liquid Flow in Horizontal Pipes," *Intl. J. Multiphase Flow* (1974) **1**, No. 1, 537-53.
16. Spedding, P.L. and Nguyen, V.T.: "Regime Maps for Air-Water Two-Phase Flow," *Chem. Eng. Sci.* (1980) **35**, No. 4, 779-93.
17. Taitel, Y. and Dukler, A.E.: "A Model for Predicting Flow Regime Transitions in Horizontal and Near Horizontal Gas-Liquid Flow," *AIChE J.* (1976) **22**, No. 1, 47-55.
18. Chisholm, D.: "Prediction of Flow Pattern Boundaries in Horizontal Two-Phase Flow," *Proc., Ind. Chem. Eng. Symposium Series* (1986) **86**, 761-72.
19. Atal, B.S.: "Automatic Recognition of Speakers From Their Voices," *Proc., IEEE* (April 1976) **64**, No. 4, 458-75.
20. Darwich, T., Toral, H., and Archer, J.S.: "An Expert System for Multiphase Measurement and Regime Identification," paper SPE 19136 presented at the 1989 SPE Petroleum Computer Conference, Lake Conroe, TX, June 23-26.



a)



b)

**Fig. 7—Comparison of actual and measured superficial velocities: (a) superficial gas velocity; (b) superficial liquid velocity.**

21. Darwich, T.: "A Statistical Method for Two-Phase Flow Metering," PhD dissertation, Imperial C., London (1989).

## SI Metric Conversion Factors

bar	$\times 1.0^*$	E+02	= kPa
cycles/sec	$\times 1.0^*$	E+00	= Hz
ft	$\times 3.048^*$	E-01	= m
in.	$\times 2.54^*$	E+00	= cm

\*Conversion factor is exact.

SPEPE

Original SPE manuscript received for review March 13, 1989. Paper (SPE 19510) accepted for publication July 3, 1990. Revised manuscript received Jan. 2, 1991.